ADVANCED HEALTHCARE MATERIALS
www.advhealthmat.de

An In Situ Curing, Shear-Responsive Biomaterial Designed for Durable Embolization of Microvasculature

*Quynh P. Pham, Jeffrey V. Groom II, Chander Sadasivan, David J. Fiorella, David C. Madoff, Lee-Jae Guo, Michael Fornaciari, Courtney Guertin, Craig Wiltsey, Lee Core, Jonathan Merlo, William Wustenberg, Renu Virmani, Adam S. Arthur, Robert S. Langer, George M. Whitesides, and Upma Sharma**

Endovascular embolization is a minimally-invasive technique whereby blood vessels supplying pathological structures are selectively occluded with various embolic agents. In many scenarios, it is desirable for the embolic to distally penetrate to the level of the microvasculature, which maximizes devascularization. Existing agents exhibit inconsistent distal penetration and have other limitations including tendency for proximal reflux, patient pain during infusion, lack of fluoroscopic radiopacity, potential for catheter adhesion, susceptibility to recanalization, and other usability challenges. NeoCast is an in situ curing, solvent-free, non-adhesive biomaterial composed of polydimethylsiloxane, bismuth trioxide, and fumed silica that possesses shear-responsive properties enabling manual injectability through commercially-available microcatheters with large and small diameter lumens. Here, embolization performance with and without flow arrest, in both arterial and venous preclinical anatomies is reported. NeoCast reproducibly achieves a rate of distal penetration with microvascular occlusion that is superior to existing agents, exhibits excellent fluoroscopic visibility, and provides durable occlusion. There is mild inflammation when NeoCast is infused into blood vessels and absence of neurotoxicity when implanted directly into brain tissue. The engineered NeoCast material is poised to become a next-generation, liquid embolic agent for applications in which distal microvascular occlusion is desired.

1. Introduction

Advances in materials science and biomaterials technology over the past few decades have enabled the development of novel medical devices that can treat a wide array of health conditions. Endovascular embolization is a minimally-invasive technique performed under fluoroscopic visualization whereby small diameter catheters are used to deliver embolic agents into targeted blood vessels to deliberately occlude blood flow. It is an essential component in the clinical management of a broad range of vascular pathologies such as the treatment of bleeding conditions and devascularization of tumors.[1,2] Embolization procedures are safe and effective in both elective and emergency settings. They are performed to augment or replace complex surgical procedures. In some applications, deep penetration of an embolic agent to the level of the microvasculature is desired in order to maximize devascularization.[3] For example, in the neuroendovascular treatment of chronic subdural hematoma, distal penetration is hypothesized to result in

Q. P. Pham, J. V. Groom II, M. Fornaciari, C. Guertin, C. Wiltsey, L. Core, J. Merlo, U. Sharma
Arsenal Medical, Inc
100 Beaver Street, Suite 302, Waltham, MA 02453, USA
E-mail: usharma@arsenalmedical.com

C. Sadasivan, D. J. Fiorella
Department of Neurological Surgery
Stony Brook Medicine
101 Nicolls Road, Stony Brook, NY 11794, USA

The ORCID identification number(s) for the author(s) of this article can be found under https://doi.org/10.1002/adhm.202404011

DOI: 10.1002/adhm.202404011

D. C. Madoff
Department of Radiology and Biomedical Imaging
Yale University
333 Cedar St., New Haven, CT 06510, USA

L.-J. Guo
CBSET, Inc
500 Shire Way, Lexington, MA 02421, USA

W. Wustenberg
Mycroft Medical LLC
20828 Ahern Blvd., Farmington, MN 55024, USA

R. Virmani
CVPath Institute Inc
19 Firstfield Rd., Gaithersburg, MD 20878, USA

A. S. Arthur
Department of Neurosurgery
University of Tennessee Health Science Center
847 Monroe Ave, Memphis, TN 38163, USA

faster resorption and/or minimization of hematoma recurrence.[4,5] In pre-operative embolization of hypervascular tumors prior to surgical resection, distal penetration results in a higher degree of devascularization which reduces intraoperative blood loss and increases the probability for complete tumor resection and subsequent tumor-free survival.[6,7] In the peripheral embolization space, deep distal penetration is desired for portal vein embolization (PVE) to induce growth of the non-embolized, non-tumor bearing liver tissue prior to resection of cancerous segments.[8] These few examples highlight the broad clinical applicability of deep distal embolization. In each of these indications, an inability to fully occlude distal vessels may allow existing collateral vessels to continue feeding pathological target tissue or inadvertently facilitate the formation of collateral vessels, both of which counteract the intended goal of the embolization procedure.[9,10]

Embolic agents that are currently utilized for deep distal penetration embolization applications include 1) particulates (e.g., polyvinyl alcohol [PVA] particles and various other polymeric microspheres), 2) ethylene vinyl alcohol (EVOH) copolymers, and 3) n-butyl cyanoacrylate (n-BCA) glues. However, these embolic materials are unable to consistently achieve penetration into small vessels. Particulates are limited in their ability to occlude distally based on the diameter of individual particles; PVA particles in particular have a tendency to aggregate, resulting in their occlusion more proximally than anticipated based on individual particle size.[11,12] EVOH copolymers, such as Onyx® (Medtronic, Inc), Squid (Balt), and Lava (Sirtex), are non-adhesive materials dissolved in dimethyl sulfoxide (DMSO) solvent. Upon injection into blood vessels, the material will precipitate and solidify due to DMSO dissipation. These agents are susceptible to premature solidification, which will block vessels proximally thereby preventing additional material from being able to proceed distally. Premature solidification will also cause material to reflux backward along the course of the microcatheter, which precludes further injection of material due to the risk of non-target embolization or catheter entrapment.[13–15] Some researchers have noted that EVOH copolymers provide more of a proximal "stump" occlusion.[14] n-BCA glues such as TRUFILL (Johnson & Johnson) are adhesive materials that rapidly polymerize when exposed to an aqueous environment. The degree of distal penetration is heavily impacted by the direction/speed of blood flow and injection technique. Researchers have found that embolization performance with n-BCA cannot be precisely controlled and as a result, distal penetration performance can be unpredictable.[16] A summary of other technical and procedural limitations of particulate, EVOH copolymer, and n-BCA embolic agents is presented in **Table 1**; for an in-depth review, please see the cited references.[17–20]

R. S. Langer
Department of Chemical Engineering
Massachusetts Institute of Technology
77 Massachusetts Avenue, Cambridge, MA 02139, USA
G. M. Whitesides
Department of Chemistry and Chemical Biology
Harvard University
12 Oxford Street, Cambridge, MA 02138, USA

There is a need for development of next-generation embolic agents with better distal penetration capability. Two in-development embolic materials are Instylla's Embrace Hydrogel Embolic System and Fluidx Medical Technology's GPX Embolic System. Embrace is a polyethylene glycol-based liquid material that forms into a soft hydrogel when injected into blood vessels; the system requires a dual-lumen catheter for delivery of the hydrogel liquid pre-cursors.[21] GPX is comprised of a low-viscosity liquid containing two oppositely charged polymers (and their associated counterions) in an aqueous solution with suspended tantalum; the polymers solidify through electrostatic condensation once in the blood environment.[22] Instylla has completed a pivotal study with Embrace while Fluidx Medical has reported technical success with GPX via a first-in-human study. Both clinical studies were for the treatment of hypervascular tumors peripherally located in the body.[23,24] It is unclear whether these materials are amenable to be used with standard, small-diameter lumen microcatheters (e.g., ≤0.018″ lumen diameter), which are typically used in neurointerventional procedures (we note that Fluidx Medical Technology is developing a separate neurovascular embolic product).

We believe that an ideal embolic agent for distal embolization should have the following characteristics: 1) Ability to provide reliable and consistent deep penetration into target vasculature; 2) Ability to achieve a durable occlusion; 3) Ability to be manually injectable through standard catheters used in both neurointerventional and peripheral embolization procedures; 4) Ability to embolize vessels in both the presence and absence of blood flow (the latter scenario is encountered in situations where the interventionalist uses a balloon occlusion catheter or implements a wedged-catheter technique in which the catheter tip is fit tightly within a vessel lumen to block blood flow); 5) Is inherently radiopaque for direct fluoroscopic visualization of the material during the embolization procedure; 6) Is compatible with computed tomography imaging (i.e., does not cause imaging artifacts); 7) Elicits a safe biological response; 8) Does not contain potentially toxic solvents or compounds; and 9) Is non-adherent to minimize risk of material adhesion to catheter resulting in entrapment or non-target embolization.

We have engineered an in situ curing, solvent-free, non-adhesive, shear-responsive biomaterial embolic agent, NeoCast, to address current limitations of existing agents used for distal penetration. In this study, we first report the in vitro material and rheological properties of NeoCast, specifically demonstrating its shear-responsive behavior and ability to be manually injectable through a range of commercially-available microcatheters. We then describe in vivo embolization performance in both the presence and absence of blood flow, wherein NeoCast exhibited enhanced distal penetration ability, durable occlusion, and excellent radiopacity properties. Finally, we show that NeoCast elicited a safe biological response in vivo in multiple anatomical locations.

2. Results

2.1. NeoCast Concept and Design

NeoCast is composed of polydimethylsiloxane (PDMS) polymers, silica filler particles, and bismuth trioxide. As depicted in **Figure 1A**, the particles of our biomaterial system interact with

Table 1. Limitations of existing embolic agents.

Particulates	EVOH	n-BCA
• Limited distal penetration based on particle diameter • Unamenable for use in absence of or retrograde to blood flow • Reliant on thrombus formation for complete occlusion • Susceptible to recanalization • Radiolucent material • Difficult to inject through smaller diameter microcatheters	• Inconsistent distal penetration • Prone to proximal reflux resulting in non-target embolization or catheter entrapment • Potential for cytotoxicity (through solvent) • Potential to cause patient pain (through solvent) • Incompatible with computed tomography (imaging artifacts) • Compatible only with solvent-resistant accessories • Variable fluoroscopic radiopacity (due to tantalum settling) • Susceptible to tantalum sparking when exposed to electro-cautery	• Inconsistent distal penetration • Strong inflammatory response • Potential to cause patient pain (through exothermic reaction) • Susceptible to non-target embolization • Susceptible to catheter adhesion

each other and PDMS to form a high-viscosity structured paste that has shear-responsive properties. When shear force is applied, the silica-silica interactions are disrupted, and the viscosity of the material drops (behaving as a fluid) temporarily and reversibly. As soon as the shear force is removed, immediate recovery of silica-silica interactions occurs, restoring the paste-like structure of the biomaterial. The shear-responsive behavior is demonstrated in Figure 1B. When a high shear of 100/s is applied to the NeoCast paste, its viscosity decreases by 500-fold but immediately recovers when a lower shear rate of 0.1/s is applied.

A separate 2-part addition cure reaction based on hydrosilylation of a vinyl-functional siloxane by a hydride-functional siloxane cross-links the material into a permanent, non-degrading solid. Once mixed together, the PDMS vinyl and hydride groups react to form carbon-carbon covalent bonds, eventually curing into a chemically cross-linked, permanent elastic solid. Images of NeoCast as a paste and cured elastomer are shown in Figure 1C. Figure 1D shows a time-course of FTIR data for mixed NeoCast material as it cures over time at 37 °C. The data illustrates consumption of the Si-H peak at 912 cm^{-1} (present in hydride PDMS) as evidence of the cross-linking mechanism. Figure S1

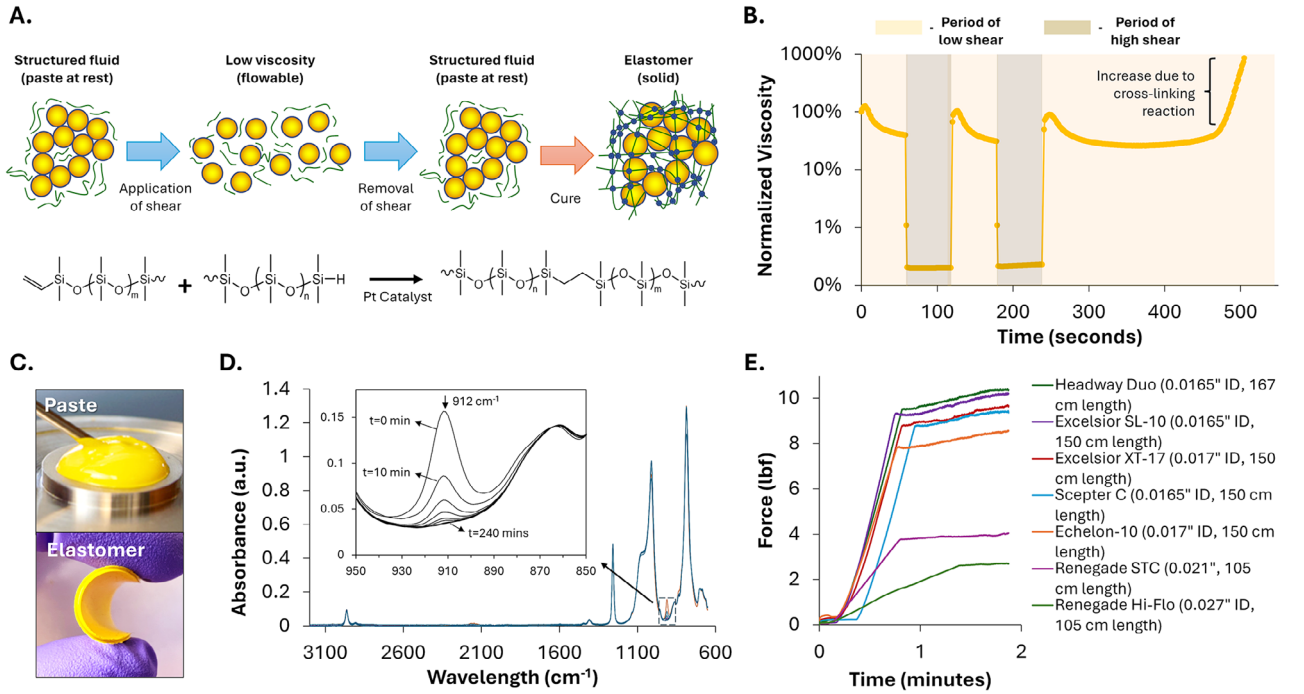

Figure 1. NeoCast design concept and injectability. A) Schematic illustrating shear-responsive behavior of NeoCast. At rest, NeoCast is a structured fluid paste with high viscosity. Upon application of shear, the particle-particle interactions are disrupted and NeoCast becomes low viscosity and flowable. When shear is removed, NeoCast returns to its initial high viscosity state. A secondary cross-linking reaction causes NeoCast to cure into a durable solid implant. B) Rheological characterization showing the shear-recovery behavior and subsequent curing reaction impact on NeoCast viscosity. When a high shear of 100/s is applied, NeoCast viscosity decreases by 500-fold and immediately recovers when a low shear of 1/s is applied. Over time, the cross-linking reaction causes the material to cure into a solid elastomer. C) Digital images of Neocast as a paste and cured elastomer material. D) FTIR analysis of mixed NeoCast material curing over time at 37 °C. The Si-H peak at 912 cm^{-1} was used to monitor the cross-linking reaction of mixed NeoCast paste material over a four-hour period. Complete consumption of the Si-H peak was observed by 90 min. E) Instron data demonstrating force required to inject NeoCast at a 0.5 mL min^{-1} rate through various neurovascular microcatheters with inner lumen diameter of ≈0.017″ is ≈10 lbf. The forces required to inject NeoCast through microcatheters with > 0.021″ lumen diameter are < 4 lbf.

(Supporting Information) shows that complete cross-linking occurs at ≈1–1.5 h. Rheological characterization indicates that the cure time at 37 and 25 °C takes 9.0 ± 0.7 and 30.1 ± 2.9 min, respectively; phase angle recovery graphs of the curing kinetics at these two temperatures are presented in Figure S2 (Supporting Information) (note that the cure time, or gel point, is the point at which the material changes from a liquid to a solid as characterized by a marked increase in viscosity; the cure time is not the same as the time it takes for complete cross-linking reaction to occur as determined by FTIR). The longer cure time at room temperature allows sufficient working time for a clinician to perform injections. As shown in Figure S3 (Supporting Information), the reaction is minimally exothermic, reaching a maximum of 37.9 ± 1.1 °C within the first 2.5 min and decreasing thereafter. NeoCast was designed to have minimal volume expansion; water displacement experiments described in Figure S4 (Supporting Information) show that NeoCast exhibits negligible volume change (measured to be 0.39 ± 1.3%) after cure. Finally, NeoCast has been confirmed to be both hemocompatible and non-cytotoxic under ISO10993 standards.[25] Complete details of this testing can be found in Tables S1 and S2 (Supporting Information), respectively.

NeoCast is supplied as a three-part phase system in small-volume syringes: there are two PDMS/bismuth trioxide suspensions (one vinyl and one hydride based) and one dry silica powder component. Bismuth trioxide is used to impart radiopacity. At the time of use, the three phases are mixed together to form the injectable paste material. As depicted in Figure S5 (Supporting Information), scanning electron microscopy analysis of cured NeoCast material shows even distribution of bismuth oxide particles, suggesting that there is homogeneous blending of material components. Packaging of silica as a separate component from PDMS is a critical design feature enabling shelf-stability of the product. As shown in Figure S6 (Supporting Information), we found that when stored together, PDMS will continually wet silica over time resulting in an inability to maintain target rheological properties upon aging. This wetting phenomenon is consistent with literature.[26]

The injection forces required to inject NeoCast at a rate of 0.5 mL min^{-1} through seven different commercial catheters are presented in Figure 1D. The forces required to inject NeoCast through five commonly used neurovascular microcatheters with lumen diameters <0.017″ were all under 10.5 lbf. We similarly tested NeoCast injection through microcatheters with larger lumen diameters and shorter lengths that are often used in peripheral embolization applications. As shown in Figure 1D, the injection force through the Renegade STC (0.021″ lumen diameter, 105 cm length) was 4.0 lbf, which is lower by a factor of ≈2.4 compared to the smaller lumen diameter microcatheters. Similarly, the injection force through the Renegade Hi-Flo (0.027″ lumen diameter, 105 cm length) was 2.7 lbf, which is lower by a factor of ≈3.6 compared to the smaller lumen diameter microcatheters.

2.2. NeoCast Exhibits Deep and Consistent Distal Penetration in the Presence of Blood Flow

The performance of NeoCast in the presence of blood flow was investigated utilizing a swine kidney embolization model. Swine kidney vasculature was selected because it is analogous to vasculature of hypervascular tumors with a capillary bed enabling an evaluation of both occlusion and distal penetration. **Figure 2** shows an example of NeoCast behavior during an embolization procedure where a microcatheter was placed within the segmental artery of the kidney. NeoCast initially exited the microcatheter as a low viscosity material that preferentially flowed into the distal vasculature (vessels with higher shear forces). As the injection continued, the material coalesced into a continuous cast that first filled the distal vessels and then proceeded more proximally. As resistance in the vessel increased and blood flow slowed, the shear rate decreased causing the material to become more viscous, providing more controlled injection and prevention of proximal reflux. The end result was a complete cast of the target vasculature. Even prior to cure (which takes 9.0 ± 0.7 min at 37 °C to complete), NeoCast exhibited sufficient structure to maintain occlusion as evidenced by lack of material movement under fluoroscopy after injections were completed. As shown in Figure S7 (Supporting Information), during the period prior to cure, NeoCast maintains the ability to behave as a fluid and could therefore be aspirated if desired by the interventionalist.

There were four animals in the NeoCast group for each of the 7-, 30-, and 90-day survival studies. Each animal received two injections: one was performed into a pole of the left kidney and the other into a pole of the right kidney. Thus, twenty-four total NeoCast injections were performed. There were three animals per timepoint for the Onyx-18 and PVA particles groups. The goal of the 90-day study was to compare the chronic tissue response to NeoCast against a commercial agent with specific indication to hypervascular tumors in the brain; Onyx-18 did not satisfy this criteria and therefore was not included in the 90-day study. Thus, twelve total Onyx-18 and eighteen total PVA particle injections were performed.

The average volume of material injected per animal was 0.8 ± 0.4 mL for NeoCast, 0.7 ± 0.4 mL for Onyx-18, and 10.5 ± 14.5 mL for PVA particles. Embolization performance was evaluated with respect to fluoroscopic radiopacity, instances of non-target embolization, and vessel occlusion performance post-embolization and at follow-up timepoints. Fluoroscopic visibility of the embolic agents was graded by the interventionalist performing the injection using a 1–5 Likert scale. As presented in **Table 2**, the fluoroscopic radiopacity of NeoCast was rated by operators to be a median of 5.0 (IQR 5.0 –5.0), which was significantly higher than median fluoroscopic radiopacity of 4.0 (IQR 3.0 – 5.0) for Onyx-18 ($p = 0.001$). The fluoroscopic radiopacity of NeoCast was also significantly higher compared to PVA particles, which had a median fluoroscopic radiopacity score of 3.0 (IQR 3.0–4.0) ($p < 0.001$).

Non-target embolization was observed in all groups, occurring most frequently with PVA particles and least frequently with NeoCast; none resulted in clinical sequelae. A summary is provided in Table 2. For PVA particles, there were a total of four instances (22%) of non-target embolization: two were due to proximal reflux that was observed during the injection via fluoroscopy while the other two instances only became apparent when discovered during histopathology of non-treated regions of the kidney. For Onyx-18, there were two instances (17%) of non-target embolization which occurred because of premature reflux around the catheter tip leading to sub-optimal distal penetration. In both

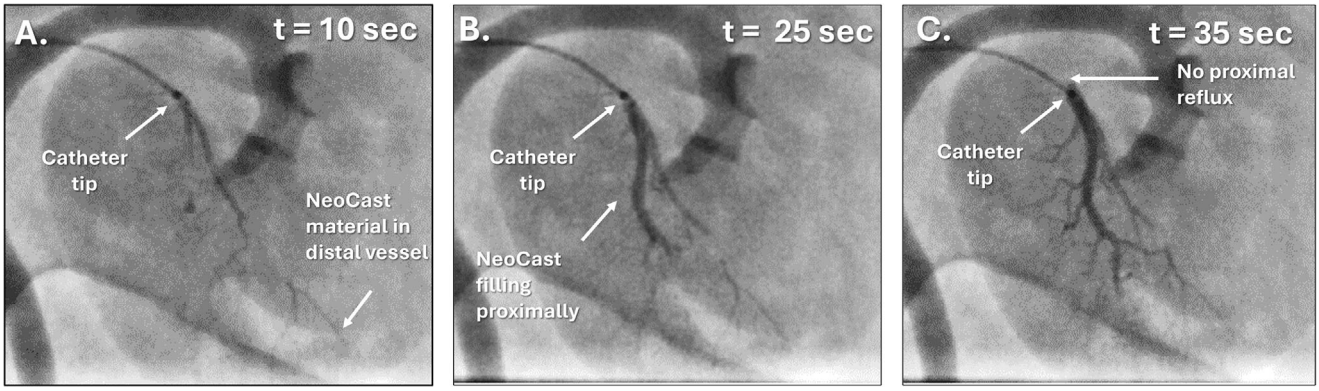

Figure 2. NeoCast embolization performance in the presence of blood flow forming a complete cast of target vasculature. A) NeoCast exits the microcatheter as a low viscosity material that preferentially flows into the distal vasculature where there are higher shear forces. B) As the injection continues, the material begins to coalesce into a continuous cast that proceeds more proximally. C) As resistance in the vessel increased and blood flow is slowed, the shear rate decreased causing the material to become more viscous, providing more controlled injection and prevention of proximal reflux. The time, t, shown in seconds for each image represents the time elapsed since the start of injection.

cases, the interventionalist attempted to continue the injection with the goal of pushing the material forward, but instead, excessive reflux occurred resulting in material flow into proximally located non-target vessels. Finally, for NeoCast, there was one instance (4%) of non-target embolization due to vessel spasm causing material to reflux into a proximal non-target vessel branch.

As assessed angiographically by the interventionalist, target vessel occlusion was considered complete for all NeoCast and Onyx-18 injections immediately post-embolization and at all follow-up timepoints. Complete occlusion was also achieved with PVA particles post-embolization but at the follow-up timepoints, there was evidence of recanalization (i.e., incomplete occlusion) in 5 of the 18 vessels, which was significantly higher when compared to NeoCast ($p = 0.030$) but not to Onyx-18 ($p = 0.197$). Representative digital subtraction angiography (DSA) images depicting NeoCast occlusion performance in the 7, 30, and 90 day experiments are shown in **Figure 3** while corresponding DSA images of Onyx-18 and PVA particles in these studies are provided in Figures S8–S10 (Supporting Information).

To assess distal penetration performance, microcomputed tomography (μCT) scanning of explanted kidneys was conducted to analyze the morphology of the vessels casted by NeoCast versus Onyx-18. As shown in **Figure 4A**, NeoCast exhibited both superior and more consistent distal performance across the injections compared to Onyx-18. A quantitative end node analysis (representing a vessel branch) of reconstructed embolic casts was performed on a representative subset of kidneys by an independent imaging core lab as a measure of distal penetration. As presented in Figure 4B, NeoCast occluded ≈5.2 times more vessel branches compared to Onyx-18 ($p = 0.006$). Further, NeoCast had a 24% variance in number of branches compared to 112% variance with Onyx-18. This result suggests better consistency and reproducibility of NeoCast embolization performance.

Since PVA particles are radiolucent, the same μCT quantitative analysis could not be performed. Instead, histomorphometry was used to characterize the distal penetration of PVA particles in comparison to NeoCast and Onyx-18. Using representative histology images, the diameters of any vessels located in the distal region of the embolized kidney were calculated based on area measurements of the vessel lumen. A box-plot of the diameter distribution for each group is shown in Figure 4C. The median diameter from an $n = 27$ vessels for PVA particles was 409 micron, which was not significantly different from a median diameter of 357 micron ($n = 13$ vessels) for Onyx-18 ($p = 0.885$); it

Table 2. Embolization performance assessment.

	NeoCast ($n = 24$ injections)	Onyx ($n = 12$ injections)	p-value (NeoCast vs Onyx)	PVA particles ($n = 18$ injections)	p-value (NeoCast vs PVA particles)
Fluoroscopic radiopacity[a)]	5 [5, 5]	4 [3, 5]	0.001	3 [3, 4]	<0.001
Instances of non-target embolization[b)]	1/24[d)] (4%)	2/12[e)] (17%)	-[g)]	4/18[f)] (22%)	-[g)]
Vessel occlusion post-embolization[c)]	Complete, 24/24	Complete, 12/12	-[g)]	Complete, 18/18	-[g)]
Vessel occlusion at follow-up timepoint[c)]	Complete, 24/24	Complete, 12/12	1.000	• Complete, 13/18 • Incomplete, 5/18	0.030

[a)] Graded on scale of 1–5 by the interventionalist at the time of injection (1 – poor; 2 – lower than average; 3 – average; 4 – good; 5 – excellent); reported as median [1st quartile, 3rd quartile]; [b)] Recorded as present or absent; [c)] Graded as complete or incomplete based on Thrombolysis in Myocardial Infarction scale; [d)] Due to proximal reflux from vessel spasm; [e)] Due to proximal reflux along microcatheter from injection; [f)] Two due to proximal reflux; two discovered during histopathology of non-treated kidney sections; [g)] No pair-wise comparisons were made since Fisher's exact test indicated no significant difference.

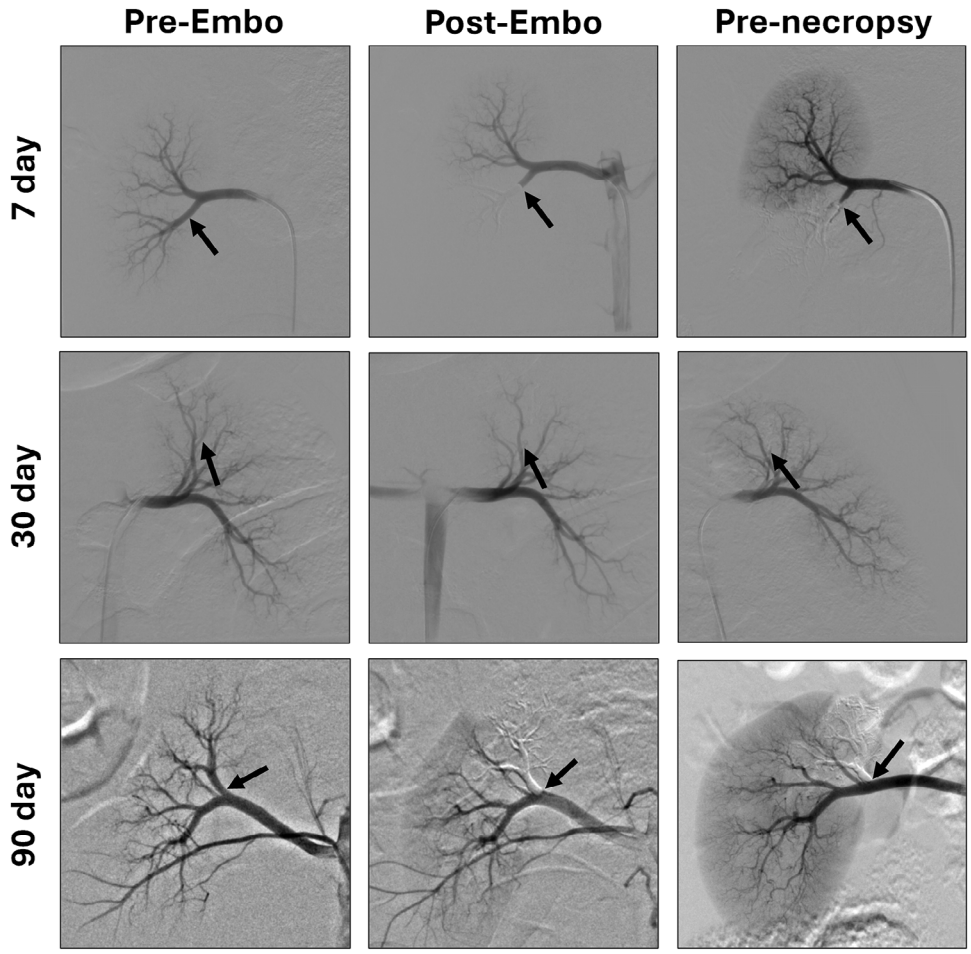

Figure 3. NeoCast embolization performance in swine kidney vasculature demonstrating a durable occlusion. Representative DSA images of kidney vasculature prior to embolization, post-embolization, and at pre-necropsy for the 7, 30, and 90 day experiments. The black arrow indicates the position of the catheter tip at the time of injection. The post-embolization images show absence of contrast flow distal to the catheter tip indicating complete occlusion is achieved. The images at follow-up also show absence of contrast flow distal to the catheter tip, indicating that complete occlusion is maintained (i.e., absence of recanalization).

was significantly larger than the median diameter of 176 micron ($n = 38$ vessels) for NeoCast ($p < 0.001$). Further analysis showed that it was more common to find NeoCast material in smaller arteries compared to PVA particles. Approximately 53% of measured vessels containing NeoCast were <200 micron in diameter compared to only 7% for PVA particles ($p < 0.001$).

We used μCT to evaluate the potential for CT artifact with NeoCast relative to Onyx. μCT images of Onyx-18 embolized kidney vasculature revealed significant streak artifact, consistent with what occurs under CT with this agent.[18] In contrast, images from NeoCast embolization exhibited minimal streak artifact. This visual difference is shown in **Figure** 5A. As shown in Figure 5B, closer inspection of the μCT data revealed that individual vessels containing NeoCast material had a homogeneous radiopaque appearance whereas vessels occluded with Onyx-18 exhibited a heterogeneous appearance. To quantify this difference, inspection of the greyscale variation within vessel areas was performed. The histogram of greyscale values for NeoCast and Onyx are displayed in Figure 5C. NeoCast shows a narrow band of pixel intensities, indicative of homogeneity. In contrast, Onyx-18 exhibits a broad range of intensities that encompasses both low and high brightness values. We attribute this variation to differences in local tantalum concentration: regions with low amounts of tantalum are dark, while those with high amounts of tantalum appear bright. The hyperdense areas of tantalum may exacerbate image artifacts on X-ray based imaging, particularly under computed tomography.[27]

2.3. NeoCast Exhibits Deep and Consistent Distal Penetration in the Absence of Blood Flow

The performance of NeoCast in the absence of blood flow was demonstrated in a swine PVE model. Clinically, PVE is a preoperative procedure performed in patients with liver cancer who require major hepatectomy. The procedure consists of embolizing the portal veins feeding tumor-bearing liver segments, in order to redirect portal blood flow to non-tumor bearing, healthy liver tissue (referred to as the future liver remnant [FLR]) causing it to grow in volume.[28,29] The degree of FLR growth, or

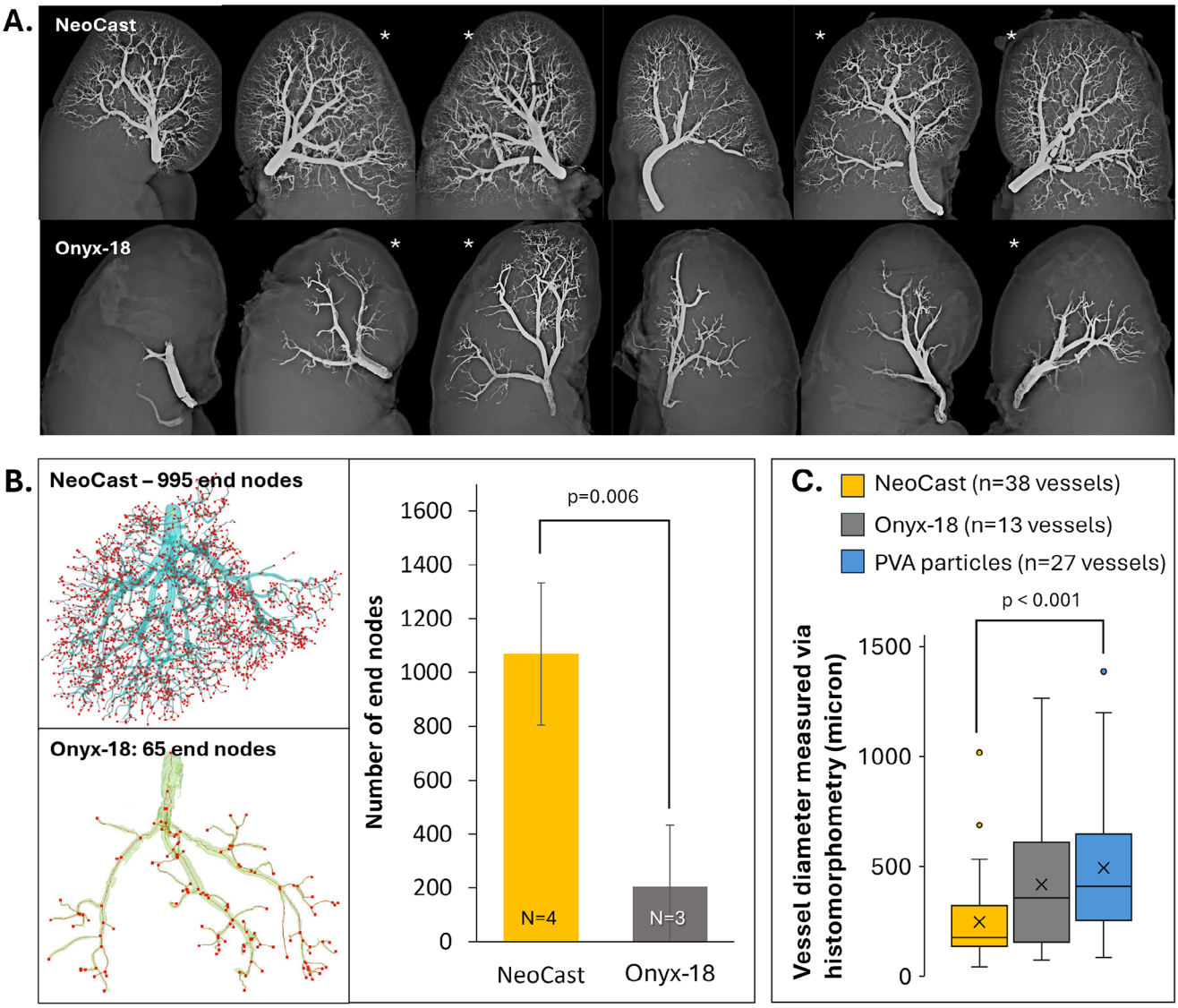

Figure 4. NeoCast exhibits consistent and deep distal penetration into target vasculature as compared to two commercial embolic agents. A) Radiograph images of swine kidneys embolized with NeoCast (n = 6, top array of panels) or Onyx-18 (n = 6, bottom array of panels). The images show superior and more consistent distal penetration achieved with NeoCast compared to Onyx-18, which was more variable. The * indicates samples that underwent quantitative analysis as shown in B and C. B) Representative 3D reconstruction of embolic casts showing end-node (representative of a vessel branch) analysis with NeoCast and Onyx-18. NeoCast significantly casts more vessels branches (> 5 times more) compared to Onyx-18. C) Box-whisker plot showing distribution of vessel diameters containing embolic material as measured histomorphometrically using images obtained from histology sections.

hypertrophy, following embolization provides a quantifiable and objective measure regarding efficacy of the procedure.

In this experiment, feasibility of NeoCast to achieve distal penetration into the portal vein vasculature was demonstrated using a balloon occlusion catheter injection technique. The control was n-BCA, which was mixed with Lipiodol in a 1:6 ratio by volume in order to impart radiopacity. **Figure** 6A shows a time-course of a representative injection with both agents. NeoCast exited the catheter and relied on the force of injection to shear-thin and be driven forward, occluding the target vasculature in a proximal to distal fashion, simultaneously casting and penetrating distal branches. In contrast, casting of vessel branches with n-BCA occurred sequentially by first occluding branches with path of least resistance and only filling other branches once pressure from the injection increased.

A total of 15 NeoCast injections were performed by a cardiovascular veterinary interventionalist across four swine. The average total amount of material injected into each swine was 14.6 ± 4.5 mL, corresponding to an exposure dose of 536 ± 152 mg kg^{-1}. There were no instances of proximal reflux resulting in NeoCast flow past the balloon proximally nor was there adhesion of material to the balloon upon microcatheter removal. A total of 10 n-BCA injections were performed into the left and left medial liver lobes of three swine with an average

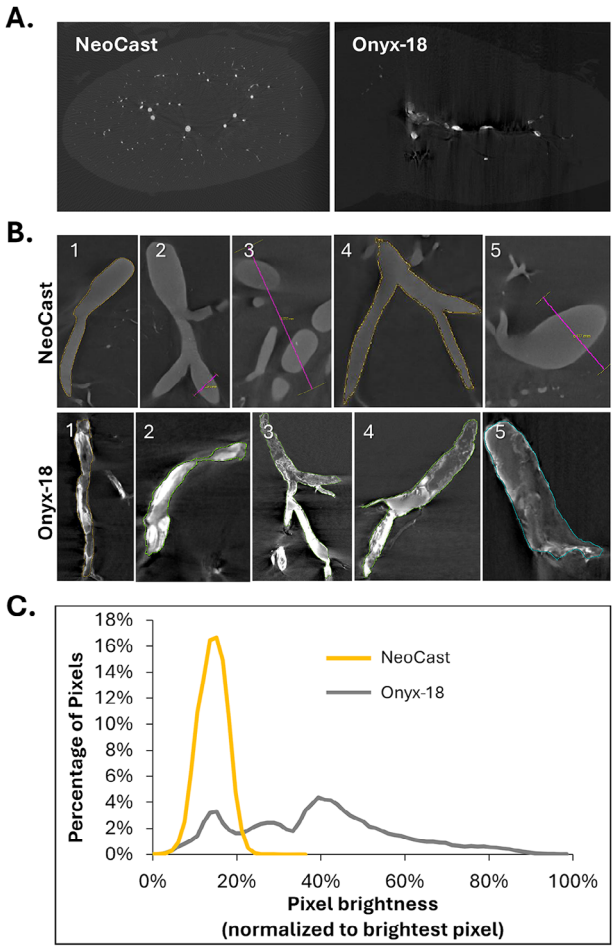

Figure 5. NeoCast exhibits homogeneous radiopacity without imaging artifact as compared to Onyx-18, a leading commercial liquid agent. A) μCT slice of embolized kidneys showing minimal streaking artifact with NeoCast compared to Onyx-18. B) μCT images of a longitudinal section of five randomly-selected embolized vessels qualitatively showing homogeneous radiopacity with NeoCast compared to heterogeneous radiopacity with Onyx-18. C) Quantitative analysis of embolic radiopacity through measurement of greyscale values of the cross sections shown in B. For each group, the data shows the percentage of pixels across all five cross sectional vessel areas as a function of pixel brightness, normalized to the brightest pixel measured (i.e., greyscale value of a pixel divided by the largest greyscale value measured); the data is weighted by the vessel area analyzed. NeoCast shows a normally distributed, narrow band of pixel brightness ranging from ≈6% – 21% with a single peak at 15% whereas Onyx-18 exhibits a multi-modal pixel brightness distribution spanning a wide range from ≈6 – 80% with local peaks at 15%, 30%, and 40% pixel brightness.

of 13.7 ± 1.7 mL material injected per swine, corresponding to an exposure dose of 329 ± 80 mg kg^{-1}. There were 2 instances (20%) of n-BCA adhesion to the balloon noted upon catheter withdrawal resulting in non-target embolization. In one instance, material was pulled into and resided within the trunk of the portal vein before becoming detached from the balloon through manual manipulation while in the other instance, material dislodged from the balloon catheter and flowed into the right (non-target) liver lobe. Figure 6B shows representative fluoroscopic images of a completed PVE procedure for both groups wherein portal vein branches feeding the left and left medial lobes were targeted for occlusion. Post-embolization DSA showed non-opacification of all NeoCast embolized vessels post-embolization indicating good occlusion was achieved. Occlusion was maintained (i.e., no recanalization) through 28 days. The digital images shown in Figure 6C highlight significant atrophy of embolized liver lobes while the FLR had rounded margins and signs of enlargement in both groups. The graph in Figure 6C depicts FLR hypertrophy as a function of absolute FLR volume increase for both groups; the degree of FLR hypertrophy for NeoCast (58% ± 31%, range 32–102%) was not significantly different from that of n-BCA (66% ± 23%, range 41–86%) ($p = 0.697$).

Figure 6D displays representative μCT images of embolic casts of NeoCast and n-BCA injected into a left medial liver lobe. Histograms of NeoCast embolic cast diameters showed that the material filled vessels ranging from 30 micron up to > 1 mm, with the majority being ≈200 micron. As shown in Figure 6E, the results were consistent across four liver lobes. The same quantitative analysis could not be performed with n-BCA because the radiopaque Lipiodol diffused into the surrounding tissue, preventing delineation of vessel structure. As a surrogate, we characterized the degree of distal penetration using histology and histomorphometry. Representative histological images presented in Figure S11 (Supporting Information) show that NeoCast was found in veins and venules with diameters as small as 25 micron whereas n-BCA was more commonly found in 200 micron diameter vessels. The average diameter of the most distal vessels containing NeoCast material observed by the histopathologist in $n = 29$ histology sections across four liver lobes was 86 ± 46 micron. In contrast, n-BCA was found by the histopathologist in larger and more centrally located veins with an average diameter of 208 ± 14 micron ($n = 10$ measurements across three liver lobes). The distribution of vessel diameters for both groups is shown in Figure S12 (Supporting Information).

2.4. NeoCast Elicits a Safe Biological Safety Response in Multiple Anatomies

2.4.1. Kidney Vasculature

The swine kidney embolization experiments provided an evaluation of arterial vascular biological safety and systemic toxicity response to NeoCast at acute and chronic timepoints. The time-course of fibrosis, inflammation, and parenchymal necrosis responses is shown in **Figure** 7A. Histological analysis of NeoCast at 7 days revealed a mild and diffuse inflammation throughout the parenchyma; fibrosis was minimal as anticipated at an acute timepoint; parenchymal necrosis was marked. Similar results were observed with PVA particles. With Onyx-18, half of the treated kidneys exhibited large areas of interstitial inflammation, resulting in a significantly higher inflammation score compared to NeoCast ($p = 0.035$) and approached significance compared to PVA particles ($p = 0.054$). NeoCast-embolized kidneys showed more calcification within the medullary region, suggesting that healing was faster than the tissues treated with the other two materials.

At 30 days, inflammation in NeoCast-treated kidneys remained unchanged relative to 7 days (i.e., mild inflammation that was

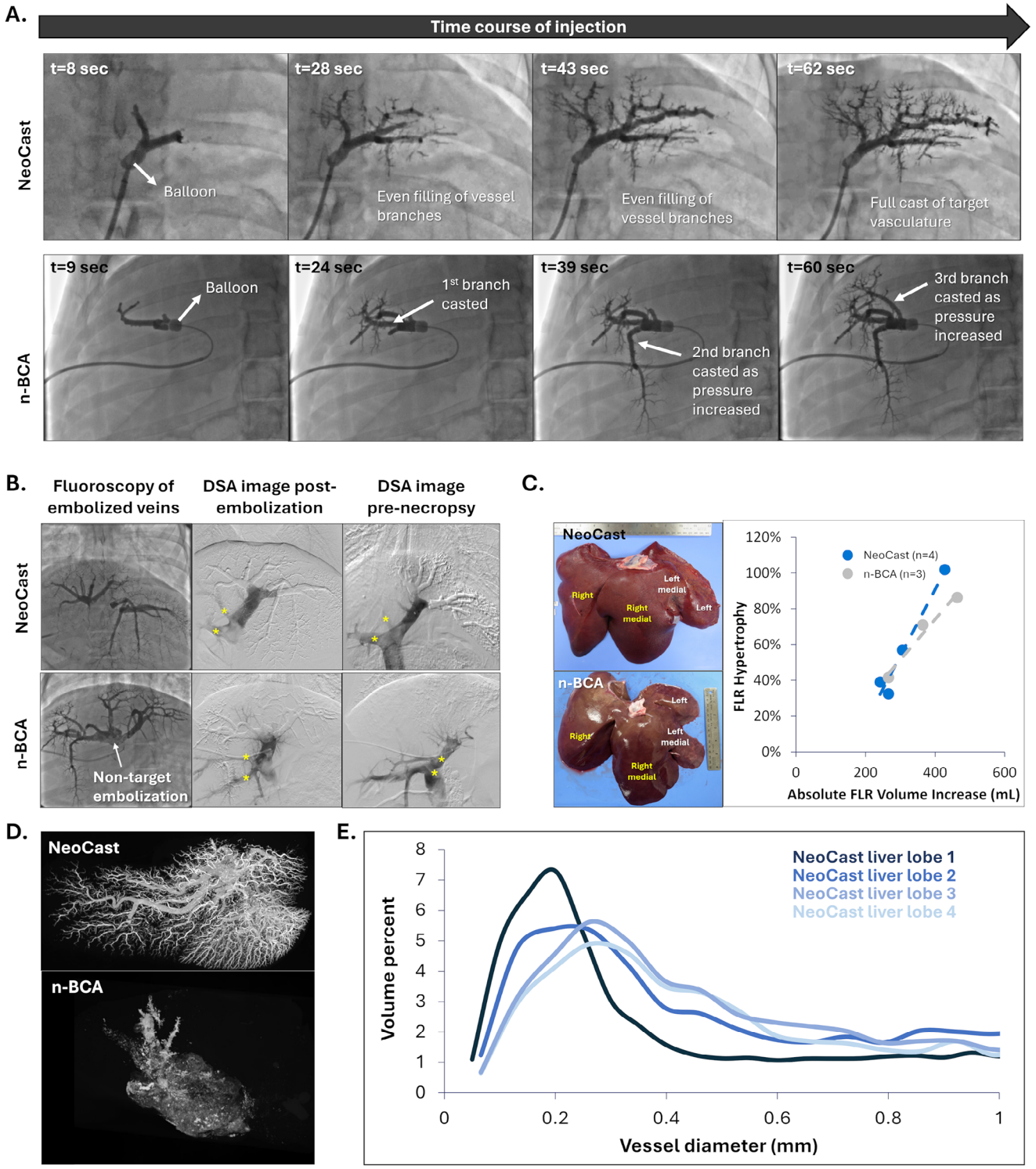

Figure 6. NeoCast and n-BCA PVE performance and outcomes. A) The top panel is a series of images showing the time-course of a NeoCast injection in which the material exits the balloon catheter and evenly fills vessel branches. The bottom panel is a series of images showing time-course of injection with n-BCA as it occludes based on the path of least resistance, resulting in sequential filling of vessel branches. The time, *t*, shown in seconds for each image represents the time elapsed since the start of injection. B) Representative images demonstrating occlusion performance with NeoCast and n-BCA. Fluoroscopic image showing the vessel branches that were embolized. In two n-BCA animals, embolic material adhered to the material during balloon withdrawal resulting in material located within the main portal vein trunk. DSA images showing occlusion of the left and left medial liver lobes post-embolization and maintenance of occlusion at 30 days. The yellow stars show contrast entering the branches supplying the right and right medial lobes. C) Evaluation of FLR hypertrophy. Gross images of explanted liver at 30 days of the right and right medial lobes (i.e., the FLR) for both NeoCast and

diffuse throughout the parenchyma). Fibrosis ranged from moderate to marked and was diffuse throughout the interstitial space; there was no necrosis in the renal parenchyma or vasculature. These results were as expected, since the treated tissue should no longer be necrotic and should be healing and organizing by 30 days. Overall, the histopathological observations were similar for PVA particles and Onyx-18, although both had an inflammation score that trended higher (but was not significant) than NeoCast. It was noted that there was more calcification in the cortex region of the kidney tissue with the Onyx-18 group, which suggests that healing was less advanced compared to NeoCast and PVA particles.

The histological response to NeoCast at 90 days remained stable relative to the 30 day timepoint, with mild inflammation, marked fibrosis, and no necrosis, which are expected responses following embolization. The local tissue response to PVA particles all scored similarly.

Examination of the histological sections also revealed a notable difference in the occlusion mechanism between NeoCast and the other embolics. As shown in Figure 7B, NeoCast completely casted the lumen vessel without the presence of any thrombus while the lumen of vessels occluded with Onyx-18 and PVA particles showed embolic material inter-mixed with thrombus (note that the empty spaces in the NeoCast sections is artifactual and due to dislodgement during histological processing, as confirmed by the histopathology lab).

Animals in this experiment were exposed to a NeoCast dose of up to 39 ± 8 mg kg^{-1}. Systemic toxicity assessments consisted of weight gain, clinical observations, clinical pathology, and gross pathology. Animal weight increases over the 7-, 30-, and 90- days were similar for all groups, and animal health remained normal throughout the study. Clinical pathology results at all time points were either within the expected range or not considered clinically significant. Gross examination of the whole body (external surface) and internal end organs (heart, spleen, lungs, liver, and regional lymph nodes) had no abnormal findings. Histopathological analysis of the heart, brain, lung, liver, spleen, and various lymph nodes from the 90 day swine experiments confirmed the absence of any embolic material in these end-organs. See Table S3 (Supporting Information) for a full listing of these histologic findings and observations.

2.4.2. Portal Vein

The swine PVE experiments provided an evaluation of venous vascular biological safety and systemic toxicity after exposure to a high dose of NeoCast. Histopathological scoring for vessel injury, endothelial loss, inflammation, and fibrosis at 30 days are shown in Figure 7C. NeoCast-embolized veins and surrounding tissue showed only a minimal amount of fibrosis and inflammation, characterized by the presence of histiocytes, giant cells, lymphocytes and eosinophils. Injury to the vascular tissue and endothelial loss were none to minimal. Examination of FLR tissue revealed healthy hepatocytes with intact lobular architecture and no abnormalities. n-BCA exhibited a relatively stronger biological response where fibrosis and inflammation were mild in severity. Interestingly, the inflammatory response was characterized by the presence of histiocytes, giant cells, and lymphocytes as well as a prominent neutrophilic component that may be indicative of an active, chronic response. n-BCA is known to contribute to a strong inflammatory response which is attributed to an exothermic reaction that can release heat as high as 80 °C.[30] Injury to the vascular tissue and endothelial loss with n-BCA were both minimal to mild. Overall, the absolute biological response to NeoCast was milder compared to n-BCA, with a standardized effect size, r, ranging from medium (e.g., $r = 0.41$ for vessel injury) to large (e.g., $r = 0.67$–0.74 for endothelial cell loss, inflammation, and fibrosis) although the differences in scores did not reach statistical significance. Representative histology images showing local tissue response to NeoCast and n-BCA are shown in Figure 7D; similar to the swine kidney experiments, NeoCast was observed to fully cast the lumen of vessels.

Animals in this experiment were exposed to a NeoCast dose of 536 ± 152 mg kg^{-1} (≈14-fold higher than in the swine kidney experiments). Systemic assessments consisted of weight gain, clinical observations, clinical pathology, and gross pathology. Animal health remained normal and weight increases were similar for both NeoCast and n-BCA groups. Clinical pathology results at all time points were either within the expected range or not considered clinically significant. Gross examination of the whole body (external surface) and internal end organs (heart, spleen, lungs, liver, and regional lymph nodes) had no abnormal findings.

2.4.3. Brain Tissue – Neurotoxicity

Although embolic agents are intended to reside within blood vessels, there are rare instances wherein vessels may rupture during an embolization procedure, in which case NeoCast would potentially contact brain tissue. To understand the brain tissue response to NeoCast, we performed neurotoxicity testing in rabbits, which consisted of injecting in situ curing material directly into brain parenchyma and evaluating animal health and local brain tissue response at 7 and 90 days. High density polyethylene was used as a negative control per ISO 10 993 part 6 Annex D guidance.[25] Neurological examinations were normal for all animals in both groups at both timepoints. At 7 days, the local tissue response to NeoCast and negative control material was nearly identical whereby sections showed a lack of polymorphonuclear cells, lymphocytes, plasma cells, macrophages, and giant cells. There was no necrosis, neovascularization, fibrosis, demyelination or fatty infiltration. At 90 days, the brain tissue response to NeoCast was benign, with absence of neuronal necrosis, absence of demyelination in a majority of implant sites, absent/minimal inflammatory cell infiltrates, and minimal

n-BCA showed enlargement while the left and left medial lobes that were embolized showed significant atrophy. The quantified degree of FLR hypertrophy was similar between NeoCast and n-BCA. D) μCT images of a left medial liver lobe embolized with NeoCast or n-BCA. Qualitatively, there is extensive casting of small vessel branches with NeoCast. Appreciation of n-BCA casting could not be determined due to dissipation of Lipiodol from within the vessel into surrounding tissue. E) Quantitative analysis of embolic cast diameter distribution showing consistent penetration achieved with Neocast in four different liver lobes.

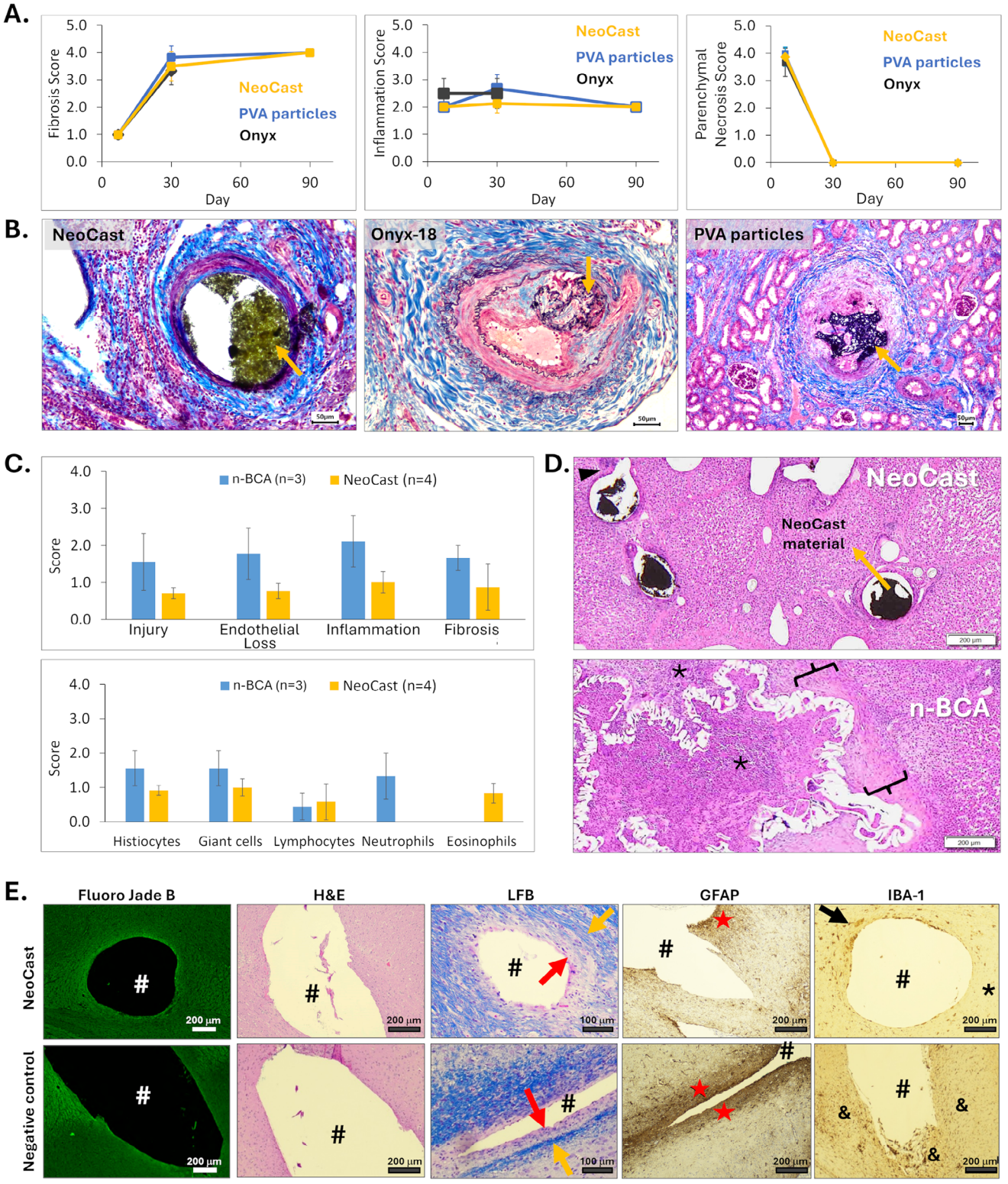

Figure 7. NeoCast elicits a safe biological response in multiple anatomical locations. A) Histopathology through 90 days in renal arteries shows a fibrotic and necrotic response that had matured and demonstrates a stable inflammatory response, which is indicative of an inert biomaterial. B) High magnification, elastic Masson Trichrome stained images of a single vessel containing embolic material, denoted by the orange arrow. The images show the presence of thrombus mixed in with Onyx-18 and PVA particles; there is no thrombus with NeoCast as the material completely fills the lumen. (Note that the area marked by the asterisk * is an artifact of histological processing which caused NeoCast material to become dislodged from the sectioned vessel lumen). C) Histopathology at 30 days in portal veins shows that NeoCast exhibited minimal inflammation, fibrosis, vessel injury and endothelial

astrocytosis and fibrosis. Representative histological images of the brain tissue response are shown in Figure 7E. Histological grading by a pathologist indicated that the brain tissue response to NeoCast was less reactive to that of the negative control. Consequently, NeoCast was assigned a reactivity grade of minimal or no reaction to brain tissue based on the grading scheme outlined in ISO 10 993 part 6 Annex E for evaluation of local response to brain implants.[25]

3. Discussion

Within the past two decades, there have been significant advances in the embolization field with the exploration of new indications, evolution of catheter technology toward smaller profiles, and development of injection techniques. The current commercially-available liquid embolic agents are based on decades-old technologies and are sub-optimal from technical, usability, safety, and efficacy standpoints. NeoCast was engineered to be a next-generation embolic agent intended for applications where deep microvascular penetration and durable occlusion are desired. Our embolic agent is a solvent-free, non-adhesive, shear-responsive PDMS-based biomaterial; it can be used with standard, small-lumen diameter microcatheters and can occlude vessels in either the absence or presence of blood flow. These are key benefits that provide interventionalists with flexibility regarding selection of microcatheters appropriate for vascular access as well as application of various injection techniques that may be required to treat different conditions based on the clinical scenario. The reliability of NeoCast to provide embolization in a controlled manner while minimizing the probability of catheter adherence, proximal reflux, and non-target embolization was demonstrated through a total of 39 successful injections across 16 swine in both arterial and venous vasculature. As a non-degrading material, NeoCast provides durable occlusion and elicits a safe biological response, including in the brain.

We selected a PDMS-based biomaterial system because silicones are commonly regarded as non-toxic, stable, and bioinert materials that have a long track record in the development of novel, biocompatible medical technologies.[31] The safety of PDMS has been controversial due to its use in breast implants, which are traditionally constructed as a cured silicone shell filled with uncured or lightly cross-linked silicone gel.[32,33] The safety concern specifically revolved around the discovery that small molecules (including low molecular weight cyclic siloxanes and platinum catalyst) from the high volumes of uncured/lightly cross-linked silicone gel diffused through the implant shell and accumulated into the surrounding tissues.[34,35] Unlike breast implants, NeoCast is a cross-linked biomaterial, similar to that of other silicone based medical devices such as finger implants, pacing leads, and facial fillers, and is therefore expected to elicit a safe biocompatibility profile.[36–38]

We developed an injectable structured fluid that exhibits both low and high viscosity properties to enable deep microvascular occlusion without crossing into the venous system. Histopathological analysis of the heart, brain, lung, liver, spleen, and various lymph nodes from our 90 day swine experiments confirmed the absence of any embolic material in these end-organs. Moreover, we have tested formulations with half the viscosity of NeoCast in swine kidney vasculature (i.e., a capillary bed) and did not see any evidence of material in veins or venules. Histopathology showed material to be present only in arteries, arterioles, and glomerular capillary loops (data not shown). Thus, the viscosity and polymerization characteristics of the NeoCast formulation were selected to ensure safety regarding non-target embolization from progression into the venous system.

The PDMS molecular weights and silica concentration were selected to ensure that NeoCast is manually injectable through standard, commercially-available microcatheters. These come in lengths varying from 75 to 175 cm long and with inner lumen diameters typically ranging from ≤ 0.018 (considered small) to 0.027 (considered large).[39] The ability to deliver viscous agents without exceeding microcatheter burst pressures becomes proportionally more difficult as the microcatheter length increases and exponentially more challenging as the inner lumen diameter decreases. Typically, microcatheters used for neurointerventional procedures are longer (≥150 cm) and have smaller inner lumen diameters (≤ 0.021) compared to those used for peripheral embolization applications.[39] We have shown that NeoCast is compatible with a number of commercial microcatheters used in neurointerventional and peripheral embolization procedures. Additionally, the forces required to inject NeoCast through these microcatheters are well within the range that can be manually generated by operators, which are 23.5 ± 3.9 and 15.9 ± 2.8 lbs by males and females, respectively.[40]

To facilitate distal penetration ability, we intentionally selected a time-based curing system, wherein the material solidifies independently of the environment. When injected into a blood vessel, NeoCast material will remain in a flowable state where it can be

loss whereas n-BCA elicited responses that were mild in severity. D) Representative hematoxylin and eosin images showing difference in occlusion and histopathologic response to NeoCast and n-BCA. NeoCast full casts vessel lumens; the arrowhead shows minimal inflammation at the periphery of a NeoCast embolized vessel. n-BCA occludes vessels mixed with thrombus; the brackets bookend a zone of fibrosis while the asterisks marks diffuse regions of inflammation with n-BCA. E) Representative images showing NeoCast biological safety response in brain tissue. The # symbol within the clear spaces of each image indicates the location of implant material. Fluoro Jade B staining shows no neuronal necrosis (characterized by absence of any fluorescence in the tissue surrounding the implant site) in both NeoCast and negative control samples. H&E staining shows an overall minimal brain tissue reaction to NeoCast. LFB staining shows a narrow band of demyelination around the NeoCast and negative control implant sites (orange arrows point to an example area of blue staining for myelin; red arrows point to areas absent of blue staining, indicating demyelination). GFAP staining showed minimal astrogliosis around the NeoCast implant site compared to a moderately thick band of astrogliosis with the negative control (the red stars indicate areas of astrogliosis, denoted by the darker brown staining). IBA-1 staining showed minimal amount of Gitter cells around the NeoCast implant site (the black arrow points to a brown stained Gitter cell while the asterisk shows a location with relatively less brown staining compared to the area near the black arrow). There was a mild amount of Gitter cells observed around the negative control implant site (the & indicates multiple sites surrounding the implant site with high density of brown staining). H&E – Hematoxylin & eosin; LFB – Luxol fast blue; GFAP – glial fibrillary acidic protein; IBA-1 – Ionized calcium-binding adaptor molecule 1.

shear-thinned (either by blood shear or through the shear from the force of injection) and be driven distally, prior to chemical cross-linking. This mechanism contrasts with solidification or polymerization mechanisms that initiate immediately upon interaction with the environment (such as with EVOH and n-BCA), which may increase the viscosity of a material too quickly resulting in reduced and/or inconsistent distal penetration into small vessels. This occurrence was observed in the swine kidney embolization experiments with Onyx-18.

A key aspect in selection of a PDMS biomaterial is its hydrophobicity relative to blood. When injected into blood vessels, the NeoCast material is predisposed to coalesce into a continuous and complete cast of the target vasculature to provide full mechanical occlusion without admixing with blood. This behavior is similar to the phase separation that occurs in an oil-in-water mixture and is supported by the histology sections of NeoCast in vessels. The ability to provide complete occlusion without requiring thrombus formation will facilitate immediate cessation of blood flow even in coagulopathic patients. Particulate-based agents are especially limited in this regard since they rely on thrombus formation within the inter-particle spaces to achieve complete occlusion.[41] Lack of thrombus may have a benefit in terms of reducing chronic inflammation since thrombus may act as a positive feedback loop for inflammatory response.[42] Further, thrombus may promote angiogenesis or resorb over time, both of which may lead to recanalization.[41] Reports of recanalization have been described in the literature for both PVA particles and EVOH copolymers.[43,44]

The biocompatibility results and histological findings in multiple different anatomical locations support our selection of PDMS as a biocompatible and bio-inert biomaterial. The independent histopathology observations through 90 days of the renal and neurological implant sites provide indirect evidence that there is no significant materials degradation or leaching of any potentially toxic compounds. In situations where degradation or leaching are present, there is typically a continued up-regulation of the local macrophage and chronic inflammatory response.[45] In many cases, the continued stimulus created by release of degradation by-products or toxic compounds will result in a mixed chronic active response. However, no such response was observed in any of our animal studies. Implant data in both renal and neurological tissues showed significant stability and/or maturation of the local histopathological response. The PVE experiments show that NeoCast is well-tolerated with no systemic toxicity even at high exposure doses.

Material radiopacity is an important attribute of embolic agents that has implications during the embolization procedure. Direct, real-time visualization of the agent during embolization is essential to appreciate the level of occlusion and to ensure absence of non-target embolization. This is especially critical in neurovascular applications where there are eloquent branches that can cause severe sequelae.[4] Due to their inherent radiolucency, particulate embolic agents do not meet this standard. While EVOH copolymers are inherently radiopaque, they are susceptible to periods of low radiopacity due to settling of the tantalum particles, which quickly occurs after product preparation.[46–48] Fluoroscopic visibility of NeoCast was consistently graded as very desirable by multiple operators. We believe that the nano size scale of the bismuth particles and viscosity of the structured NeoCast paste material reduce the degree of particle settling. As a result, the bismuth particles remain homogeneously distributed throughout the polymer matrix. This provides enhanced fluoroscopic radiopacity as well as prevention of imaging artifacts, both of which were shown by the μCT data. We expect similar compatibility with regular CT imaging.

Our extensive pre-clinical data demonstrates NeoCast embolization performance (e.g., radiopacity, distal penetration, occlusion, reflux, non-target embolization, catheter adhesion) and biological safety in pre-clinical models. The next developmental milestone is to initiate testing in human subjects, which will be required to ascertain the potential advantages of NeoCast regarding clinical outcomes compared to existing agents. Results of the PVE model provide initial evidence of performance whereby embolization with NeoCast led to a clinically meaningful outcome: induction of a high level of FLR hypertrophy on par with n-BCA but with a milder inflammatory response. We selected n-BCA as a comparator because this agent has been shown preclinically and clinically to induce the highest degree of FLR hypertrophy compared to other embolics such as PVA particles.[49–51] Nevertheless, due to the technical challenges of working with n-BCA, many physicians elect to perform PVE with particulate agents because they are easier to use despite inducing sub-optimal levels of FLR hypertrophy. Thus, if our preclinical results translate to the clinic, NeoCast could become an ideal embolic agent for a PVE indication.

4. Conclusion

In summary, we have developed an in situ curing, solvent-free, non-adhesive, shear-responsive embolic agent that can be injected through small-lumen diameter microcatheters to embolize vessels either in the presence or absence of blood flow. NeoCast is designed to be an easy-to-use agent allowing interventionalists to provide embolization in a controlled manner without minimal risk of proximal reflux and non-target embolization. NeoCast exhibits excellent radiopacity properties for fluoroscopic visualization and is expected to have CT compatibility. As a non-degrading material, NeoCast provides durable occlusion and elicits a safe biological response, including in the brain. Overall, the results highlight the promising potential for NeoCast to be an ideal, next-generation embolic for applications where deep microvascular penetration and permanent occlusion is desired. In particular, the excellent biocompatibility of NeoCast along with injectability through small-diameter lumen microcatheters makes the material uniquely suited for neuroendovascular applications. The next step is to demonstrate translation of the preclinical results into the clinic. Success would significantly advance the endovascular embolization field by providing interventionalists with an easy-to-use embolic agent to safely provide deep and durable occlusion.

5. Experimental Section

Study Design: The overall study was designed to evaluate NeoCast embolization performance and biological safety in different preclinical models. Embolization performance relative to commercial embolic agents was evaluated in both the presence and absence of blood flow. Embolization performance in the presence of blood flow was evaluated using a swine

kidney embolization model. Timepoints for these experiments were 7, 30, and 90 days. Primary endpoints were distal penetration and biological safety response. Embolization performance in the absence of blood flow was evaluated using a swine liver portal vein embolization model. The timepoint for this experiment was 30 days, with the primary endpoints being FLR hypertrophy and biological safety response. In both models, additional assessments were recorded including occlusion performance, presence of reflux, presence of non-target embolization, and fluoroscopic radiopacity. Distal penetration performance was quantified using μCT analysis of embolic casts of occluded vasculature. Neurotoxicity testing in rabbits was also conducted to evaluate biological safety response to NeoCast when directly exposed to brain tissue (as a worse-case scenario in case of vessel rupture during a procedure). Timepoints for neurotoxicity evaluation were 7 and 90 days.

NeoCast Manufacturing and Testing: The components of the proprietary NeoCast formulation consist of vinyl and hydride PDMS, catalyst, catalyst modifier, bismuth trioxide, and fumed silica. NeoCast was manufactured as three individual phases stored individually in 5 mL syringes. Once the individual phase syringes were prepared, they undergo an annealing step. For animal experiments, the syringes were subjected to E-beam sterilization (Steritek, Fremont, CA). To prepare NeoCast for subsequent use (e.g., rheological analysis, injection force testing, animal studies etc.), the three phases were homogeneously mixed, resulting in a paste material. Performance of the NeoCast was tested via rheological characterization at 37°C using a TA Instruments DHR-1 rheometer (New Castle, DE) with a Peltier plate geometry. Cure time (or gel point) was determined using an oscillation time sweep; the cure time was defined as when the phase angle reached a local maximum. Shear-recovery testing was conducted by subjecting the paste to alternating intervals (duration of 60 s) where low and high shear rates, respectively, were applied. A final shear rate was then applied until the material cured. Temperature of NeoCast during the curing reaction was measured by a thermocouple placed within sample material that had been injected inside a 2 mm tube and submerged in a 37°C water bath. FTIR (Perkin Elmer Spectrum 100) was performed on samples of NeoCast material prepared from a single device that had been placed in a 37 °C oven for 0, 10, 20, 30, 45, 60, 90, 120, 150, 180, or 240 min (for time 0 min, the sample was directly deposited onto the attenuated total reflectance crystal). The samples were analyzed between 4000 and 650 cm^{-1}. The Si-H peak at 912 cm^{-1} (present in hydride PDMS) was used to monitor the reaction. The band located at 864 cm^{-1} attributed to the Si–C stretching vibration of PDMS Si–CH_3 groups was used to normalize spectra relative to the t = 0 spectrum.[52]

Instron Injection Force Characterization: The force required to inject NeoCast through various microcatheters (Echelon-10, Medtronic, Minneapolis, MN; Excelsior SL-10 and Excelsior XT-17, Stryker, Kalamazoo, MI; Headway Duo and Scepter C, MicroVention, Inc., Aliso Viejo, CA; Renegade HI-FlO and Renegade STC, Boston Scientific, Marlborough, MA) was assessed using an Instron (Model 3340). A 1 mL syringe filled with NeoCast material was connected to a microcatheter and then orientally vertically within a custom fixture, which allowed depression of the syringe plunger by the upper plate of the Instron. Testing was conducted at a crosshead speed of 0.5 mL min^{-1}. The force on the plunger was measured using a 50 N load cell and recorded using Bluehill version 3 software.

Swine Kidney Embolization Experiments: The 7 and 30 day swine kidney embolization experiments were conducted at Stony Brook University while the 90 day experiments were conducted at CBSET, Inc. (Lexington, MA) under Good Laboratory Practice (GLP) conditions. Both sites were assured by the Office of Laboratory Animal Welfare and accredited by AAALAC; all experiments were conducted after obtaining Institutional Animal Care and Use Committee (IACUC) approval at the respective institutions. Female and male Yorkshire swine (*Sus scrofa domesticus)* 34.6–44.6 kg were used. Animal health and clinical pathology were assessed at various timepoints throughout the respective in-life period.

The experimental design consisted of an $n = 4$ animals for the NeoCast group and an $n = 3$ animals for Onyx-18 (Medtronic, Minneapolis, MN) and PVA particles groups (90–180 micron diameter, Cook Medical, Bloomington, IN). Access to the renal arteries was obtained through the femoral artery. Standard interventional techniques were used to guide microcatheters to target vessel branches. In the 7 and 90 day experiments, the microcatheter tip was placed proximally within the renal vasculature within a segmental artery to occlude a single pole of the kidney. In the 30 day experiments, the microcatheter tip was placed more distal within the renal vasculature within a interlobar artery, resulting in a more selective occlusion. For each animal, the same embolic was used to occlude both kidneys so that systemic effects could be attributed. NeoCast and Onyx-18 were injected using an Echelon-10 microcatheter while PVA particles were injected using a Progreat 2.4 Fr microcatheter (Terumo, Somerset, NJ). Fluoroscopic videos and digitally subtracted angiography were obtained for all injections and at pre-necropsy to determine occlusion performance, which was graded using the Thrombolysis in Myocardial Infarction scale: 0 – Absence of any antegrade flow beyond target occlusion (no perfusion); 1 – Any faint antegrade flow beyond target occlusion, with incomplete filling of distal branches (penetration without perfusion); 2 – Delayed or sluggish antegrade flow with complete filling of some distal branches (partial perfusion); and 3 – Normal flow that fills all distal branches (complete perfusion).[53] A score of 0 or 1 was considered complete occlusion whereas a score of 2 or 3 was considered incomplete occlusion. Fluoroscopic radiopacity was graded by the interventionalist on a scale from 1–5 (1 – poor; 2 – lower than average; 3 – average; 4 – good; 5 – excellent). Non-target embolization caused by material reflux during active injection or during catheter removal as a result of dislodgement of adhered material was marked as absent or present. At necropsy, the kidneys were explanted and placed in formalin for μCT scanning and subsequent histological analysis, which consisted of evaluating the degree of inflammation, fibrosis, and parenchymal necrosis. Sections were scored by an independent histopathologist (CVPath Institute, Gaithersburg, MD) based on a 0–4 scale (0 – none, 1 – minimal, 2 – mild, 3 – moderate, 4 – marked). In the 90 day experiment, end organs including the heart, brain, skin, lung, liver, adrenal glands, spleen, retropharyngeal lymph nodes, aortic lymph nodes, mesenteric lymph nodes, and sternum were also evaluated histologically.

Distal penetration of NeoCast and Onyx-18 embolic casts was quantified by Synopsis Inc. (Sunnyvale, CA) using SimpleWare software using an end-node analysis. First, 3D volumes of the embolic casts were segmented from the μCT data followed by centerline network generation. Termination of a centerline was identified as an end node, which represents a vessel branch. The distribution of vessel diameters infused with NeoCast, Onyx-18, and PVA particles was assessed histomorphometrically by measuring the diameters of any vessels containing embolic material. Radiopacity analysis was also performed by Synopsys through inspection of the greyscale variation within a vessel area from a 2D μCT image slice. A histogram of the greyscale values was provided.

Swine PVE Experiments: The PVE experiments were performed at CBSET after obtaining IACUC approval. Male and female Yorkshire swine (*Sus scrofa domesticus)* 36.1–40.3 kg were used. Animal health and clinical pathology were assessed at various timepoints throughout the in-life period.

The experimental design consisted of an $n = 4$ animals for NeoCast and an $n = 3$ animals for n-BCA. Transhepatic access to the portal vein for embolic injections was obtained percutaneously through the right liver lobe under fluoroscopic guidance. Interventional techniques were used to guide a 9 mm balloon catheter (4 Fr Fogarty Thru-Lumen Embolectomy Catheter, Edwards Lifesciences) to the portal vein branches supplying blood to the left and left medial liver lobes. Upon confirmation of cessation of blood flow distal to the site of balloon inflation, material was injected. For NeoCast, the balloon was left inflated until material cure and then deflated and withdrawn. For n-BCA, upon completion of injection, the balloon was carefully deflated and expeditiously withdrawn to minimize risk of material adhesion. Fluoroscopic videos and digitally subtracted angiography were obtained for all injections and prior to necropsy to determine occlusion performance. Animals were euthanized 30 days following the embolization procedure. The liver was then explanted, photographed, and the individual lobes were separated, weighed, and stored in 10% formalin. The left medial lobe of each animal was sent to Micro Photonics Inc. (Allentown, PA) for μCT scanning and diameter distribution of embolic casts. Histopathology of both embolized and non-embolized

liver segments were performed at CBSET, Inc. The degree of vessel injury, endothelial loss, fibrosis, and overall inflammation, including the specific cell types (i.e., histiocytes, giant cells, lymphocytes, neutrophils, and eosinophils) were graded on a 0–4 scale (0 – none, 1 – minimal, 2 – mild, 3—moderate, and 4 – marked). Additionally, for each section analyzed, the diameter of the smallest vessel containing embolic material was recorded by the histopathologist.

Animals underwent CT imaging in a SIEMENS Biograph 6 scanner (Munich, Germany) of the liver at baseline prior to embolization and prenecropsy. Animals were scanned during a period of breath cessation to minimize imaging artifact. The length of each non-breathing session was equivalent to the length of the scan, ≈60 s. The CT scans were used by PIA Medical (Bellevue, WA) to create 3D constructs of the liver and subsequently segmented into individual liver lobes. Liver lobes were segmented utilizing landmarks such as the gallbladder, hepatic veins, portal veins, and embolic material). FLR hypertrophy was calculated as:

$$(FLR_{30day} - FLR_{baseline})/FLR_{baseline} \times 100 \quad (1)$$

Neurotoxicity: The neurotoxicity experiments were performed at North American Science Associates (Minneapolis, MN) after obtaining IACUC approval. New Zealand White rabbits weighing between 2.5–3.5 kg were used. The experiments were designed to evaluate biological response of brain tissue to NeoCast relative to a negative control (high density polyethylene rods). Briefly, an incision was made through the skin over the dorsal midline of the cranium. The fascia and muscles were cut and reflected to expose the cranium. The skin, underlying fascia, and periosteum over the cranium were then reflected to expose the cranial bone at two target sites of the right hemisphere of the cranium spaced 1 cm apart. At each target site, a circular defect was made using a 2–4 mm burr drill. The defect sites were irrigated with saline to remove bone particles. An appropriately sized dural incision was created centrally within each craniotomy defect. For each animal, either NeoCast or the negative control was implanted at both sites. With NeoCast, ≈20 microliters of material was injected through the dural incision into the brain parenchyma using a needle. The negative controls (1 mm diameter x 6 mm length, volume = ≈4 microliters) were directly inserted into the parenchyma. The 7- and 90- day experiments evaluated an $n = 4$ and $n = 8$ implant sites, respectively, for each group. An equal number of male and female rabbits were used for each group.

Endpoints consisted of overall animal health (neurological exams) and histopathology. Physiological and neurological examinations were performed by a veterinarian at baseline and periodic intervals through study timepoints. Histopathology consisted of examination of implantation sites and draining lymph nodes. Sections underwent hematoxylin & eosin, Luxol Fast Blue, glial fibrillary acidic protein, ionized calcium-binding adaptor molecule 1, and/or Fluoro Jade B staining. Scoring was based on the guidelines described in ISO10993-6 Annex E – Examples of evaluation of local biological effects after [brain] implantation. Briefly, the presence of inflammatory cell infiltrates, necrosis, and overall tissue response (e.g., neovascularization, fibrosis, astrocytosis, demyelination) from a section of each implant site were assessed on a 0 – 4 scale. The scores were totaled and a group average calculated. The average score for the negative control was subtracted from that of the NeoCast group to determine a reactivity grade based on the following scale: 0.0–2.9 = minimal or no reaction; 3.0–8.9 = slight reaction; 9.0–15.0 = moderate reaction; >15 = severe reaction.

μCT: Explanted organs underwent μCT scanning at Micro Photonics, Inc. (Allentown, PA) to create high-resolution 3D images of the embolized vasculature. Scanning was performed using a SkyScan 1273 at a voxel size of 33 micron and image size of 3072 × 1944 pixels. Parameters for scanning were 110 kV, 300 μA, 94 ms exposure time, and 0.3 degrees rotation step.

Statistical Analysis: Continuous variables were reported as mean ± standard deviation or median based on normality. Discrete variables were summarized using percentage. For normally distributed data sets, Welch's t-test was used to determine significance between two groups with unequal sample size. For non-normal data, Mann-Whitney U test was used to compare between two groups while Kruskal-Wallis method with Dunn's multiple comparisons was used to compare between three groups. Fisher's exact test was used to compare counts of events between groups. A p-value <0.05 was defined as significant for all tests; p-values were adjusted using the Bonferroni method for multiple comparisons when warranted. Statistical analysis was performed using R version 4.4.0 (Vienna, Austria).

Supporting Information

Supporting Information is available from the Wiley Online Library or from the author.

Acknowledgements

The authors thank Gareth McKinley for his assistance with rheological characterization methods. The authors also thank Changcheng You for his assistance with FTIR characterization methods. Q.P.P., J.V.G., M.F., C.S., C.G., C.W., L.C., J.M., and D.J.F. acknowledge funding from the National Cancer Institute grant R44CA257802. Q.P.P., J.V.G., M.F., C.W., and D.C.M. acknowledge funding from the National Heart, Lung, and Blood Institute grant R43HL15486.

Conflict of Interest

Q.P.P., J.V.G., M.F., C.G., C.W., L.C., J.M., and U.S. are current or former employees of Arsenal Medical and own stock options in the company. U.S. is the President and CEO and L.C. is the Chief Operating Oficcer of Arsenal Medical. J.V.G, C.W., Q.P.P., C.G., L.C., and U.S are inventors on embolic patents that have been issued/allowed/pending. C.S. has received research support from Medtronic Neurovascular and Arsenal Medical. D.J.F is a consultant for, has received research support, and has stock options in Arsenal Medical. He has recieved consulting, proctoring, and research support from Medtronic Neurovascular. He has received traivel, consulting, and research support from Balt USA. He reports compenstation from Johnson & Johnson Health Care Systems, Inc. for consultant services. D.C.M. receives consulting fees from Boston Scientific, Arsenal Medical, and participates on the data safety monitoring board of Sirtex. A.SA. is a consultant for and has stock options in Arsenal Medical. He is a consultant for Balt USA, Johnson & Johnson, and Medtronic. He also has research support from Balt USA and Medtronic. R.S.L. and G.M.W. are co-founders of and have stock/stock options in Arsenal. W.W. and R.V. declare they have no competing interests.

Author Contributions

Q.P.P., J.V.G., C.S., D.J.F., D.M., U.S., and A.A. performed conceptualization. Q.P.P., J.V.G., C.S., R.V., and W.W. performed formal analysis. Q.P.P., J.V.G., D.J.F., L.C., W.W., A.A., G.M.W., and U.S. performed funding acquisition. Q.P.P., J.V.G., L.G., M.F., C.S., C.G., C.W., J.M., and D.J.F. performed investigation. Q.P.P., J.V.G., L.G., J.M., L.C., and U.S. performed project administration. Q.P.P., J.V.G., D.J.F., D.C.M., L.C., and U.S. performed supervision. Q.P.P. and J.V.G. performed wrote the original draft preparation. Q.P.P., J.V.G., C.S., D.J.F., D.C.M., R.S.L., and U.S. performed wrote, reviewed, and edited the draft.

Data Availability Statement

The data that support the findings of this study are available from the corresponding author upon reasonable request.

Keywords

biomaterial, embolic, microvascular, occlusion, shear-responsive

Received: October 16, 2024
Revised: January 31, 2025
Published online:

[1] E. J. Duffis, C. D. Gandhi, C. J. Prestigiacomo, T. Abruzzo, F. Albuquerque, K. R. Bulsara, C. P. Derdeyn, J. F. Fraser, J. A. Hirsch, M. S. Hussain, H. M. Do, M. V. Jayaraman, P. M. Meyers, S. Narayanan, *J. Neurointerv. Surg.* **2012**, *4*, 251.
[2] J. Golzarian, M. R. Sapoval, S. Kundu, D. W. Hunter, E. N. Brountzos, J.-F. H. Geschwind, T. P. Murphy, J. B. Spies, M. J. Wallace, T. de Baere, J. F. Cardella, *J. Vasc. Interv. Radiol.* **2010**, *21*, 436.
[3] M. Lubarsky, C. Ray, B. Funaki, *Semin. Intervent. Radiol.* **2010**, *27*, 099.
[4] D. Fiorella, A. S. Arthur, *J. Neurointerv. Surg.* **2019**, *11*, 912.
[5] J. S. Catapano, A. F. Ducruet, C. L. Nguyen, J. F. Baranoski, T. S. Cole, N. Majmundar, D. A. Wilkinson, V. L. Fredrickson, D. D. Cavalcanti, F. C. Albuquerque, *J Neurointerv. Surg.* **2021**, *13*, 657.
[6] D. M. Raper, R. M. Starke, F. Henderson Jr., D. Ding, S. Simon, A. J. Evans, J. A. Jane Sr., K. C. Liu, *AJNR Am. J. Neuroradiol.* **2014**, *35*, 1798.
[7] J. S. Catapano, A. C. Whiting, A. W. Mezher, C. J. Przybylowski, A. P. See, M. A. Labib, V. L. Fredrickson, D. D. Cavalcanti, M. T. Lawton, A. F. Ducruet, F. C. Albuquerque, N. Sanai, *World Neurosurg.* **2020**, *135*, 679.
[8] T. de Baere, A. Denys, D. C. Madoff, *Tech. Vasc. Interv. Radiol.* **2007**, *10*, 67.
[9] R. Avritscher, T. de Baere, R. Murthy, F. Deschamps, D. C. Madoff, *Semin. Intervent. Radiol.* **2008**, *25*, 132.
[10] A. Perry, M. R. Chicoine, E. Filiput, J. P. Miller, D. T. Cross, *Cancer* **2001**, *92*, 701.
[11] J. Carnevale, G. Kocharian, J. Goldberg, A. Ramos, J. Schwarz, J. Knopman, *Endovasc. Today* **2021**, *20*, 66.
[12] J. Golzarian, L. Weng, *J. Vasc. Interv. Radiol.* **2014**, *25*, 1773.
[13] M. Shapiro, M. Walker, K. T. Carroll, M. R. Levitt, E. Raz, E. Nossek, N. Delavari, O. Mir, P. K. Nelson, *J. Neurointerv. Surg.* **2021**, *13*, 471.
[14] T. W. Link, S. Boddu, S. M. Paine, H. Kamel, J. Knopman, *Neurosurgery* **2019**, *85*, 801.
[15] J.-S. Oh, S.-M. Yoon, J.-J. Shim, H.-G. Bae, *J. Korean Neurosurg. Soc.* **2015**, *57*, 54.
[16] H. Hill, J. F. B. Chick, A. Hage, R. N. Srinivasa, *Diagn. Interv. Radiol.* **2018**, *24*, 98.
[17] Y. Takeuchi, H. Morishita, Y. Sato, S. Hamaguchi, N. Sakamoto, H. Tokue, T. Yonemitsu, K. Murakami, H. Fujiwara, K. Sofue, T. Abe, H. Higashihara, Y. Nakajima, M. Sato, *Jpn J. Radiol.* **2014**, *32*, 500.
[18] D. F. Vollherbst, R. Chapot, M. Bendszus, M. A. Möhlenbruch, *Clin. Neuroradiol.* **2022**, *32*, 25.
[19] J. Lord, H. Britton, S. G. Spain, A. L. Lewis, *J. Mater. Chem. B* **2020**, *8*, 8207.
[20] M. Guimaraes, D. Arrington, T. MacFall, R. Yamada, C. Schonholz, *Endovasc. Today* **2013**, 70.
[21] S. Ganguli, R. Lareau, T. Jarrett, M. C. Soulen, *J. Vasc. Interv. Radiol.* **2021**, *32*, 813.
[22] R. J. Stewart, M. Sima, J. Karz, J. P. Jones, *Front. Bioeng. Biotechnol.* **2023**, *11*, 1095148.
[23] G. S. Goh, M. D. Goodwin, J.-F. Huang, H. Kavnoudias, A. Holden, *J. Vasc. Interv. Radiol.* **2022**, *33*, 660.
[24] A. Holden, M. Krauss, R. O'Hara, J. Jones, D. K. Smith, *J. Vasc. Interv. Radiol.* **2024**, *35*, 232.
[25] *ISO 10993–6* Biological evaluation of medical devices Part 6: Tests for local effects after implantation, **2016**.
[26] J. V. DeGroot Jr., C. W. Macosko, *J. Colloid Interface Sci.* **1999**, *217*, 86.
[27] K. M. Treitl, M. Scherr, M. Forth, F. Braun, D. Maxien, M. Treitl, *Eur. Radiol.* **2015**, *25*, 597.
[28] D. Li, D. C. Madoff, *Cancer Biol. Med.* **2016**, *13*, 426.
[29] B. J. May, D. C. Madoff, *Semin. Intervent. Radiol.* **2012**, *29*, 81.
[30] P. O. Comby, K. Guillen, O. Chevallier, M. Lenfant, J. Pellegrinelli, N. Falvo, M. Midulla, R. Loffroy, *J. Clin. Med.* **2021**, *10*, 4320.
[31] M. Zare, E. R. Ghomi, P. D. Venkatraman, S. Ramakrishna, *J. Appl. Polym. Sci.* **2021**, *138*, 50969.
[32] A. U. Daniels, *Swiss Med. Wkly* **2012**, *142*, w13614.
[33] D. Downing, *J. Nutr. Environ. Med.* **1998**, *8*, 317.
[34] D. Flassbeck, B. Pfleiderer, P. Klemens, K. G. Heumann, E. Eltze, A. V. Hirner, *Anal. Bioanal. Chem.* **2003**, *375*, 356.
[35] M. A. Brook, *Biomater* **2006**, *27*, 3274.
[36] BioPro. Digitalis Silicone Spacer, https://bioproimplants.com/portfolio-view/digitalis-silicone-spacer (accessed: January 2025).
[37] Surgiform. Silicone Facial Implants, https://surgiform.com/silicone-implants/ (accessed: January 2025).
[38] Medtronic. Capsure Pacing Leads Family, https://www.medtronic.com/en-us/healthcare-professionals/products/cardiac-rhythm/pacing-systems/pacing-leads-delivery-systems/capsurefix-novus-mri-surescan-pacing-lead.html (accessed: January 2025).
[39] P. J. Patel, Q. S. Kelly, *Endovasc. Today* **2014**, 38.
[40] A. Harth, W. R. Vetter, *Occup. Ther. Int.* **1994**, *1*, 13.
[41] R. A. Sheth, S. Sabir, S. Krishnamurthy, R. K. Avery, Y. S. Zhang, A. Khademhosseini, R. Oklu, *J. Funct. Biomater.* **2017**, *8*, 12.
[42] K. Stark, S. Massberg, *Nat. Rev. Cardiol.* **2021**, *18*, 666.
[43] H. Chihara, H. Imamura, T. Ogura, H. Adachi, Y. Imai, N. Sakai, *NMC Case Rep. J.* **2014**, *1*, 1.
[44] S. K. Natarajan, D. Born, B. Ghodke, G. W. Britz, L. N. Sekhar, *J. Neurosurg.* **2009**, *111*, 105.
[45] J. M. Anderson, *Cardiovasc. Pathol.* **1993**, *2*, 33.
[46] R. Duran, K. Sharma, M. R. Dreher, K. Ashrafi, S. Mirpour, M. Lin, R. E. Schernthaner, T. R. Schlachter, V. Tacher, A. L. Lewis, S. Willis, M. den Hartog, A. Radaelli, A. H. Negussie, B. J. Wood, J. F. Geschwind, *Theranostics* **2016**, *6*, 28.
[47] Y. Y. Jiang, Y. E. Jo, J. M. Woo, O. K. Lim, C. Hwang, J. Y. Maeng, J. Kim, N. Kim, D. H. Lee, *Neurointervention* **2017**, *12*, 3.
[48] J. R. Mason, C. Dodge, G. Benndorf, *Interv. Neuroradiol.* **2018**, *24*, 574.
[49] B. Guiu, P. Bize, D. Gunthern, N. Demartines, N. Halkic, A. Denys, *Cardiovasc. Intervent. Radiol.* **2013**, *36*, 1306.
[50] T. de Baere, A. Denys, V. Paradis, *Eur. Radiol.* **2009**, *19*, 1435.
[51] J. H. M. Luz, F. Veloso Gomes, N. V. Costa, I. Vasco, E. Coimbra, P. M. Luz, H. P. Marques, J. S. Coelho, R. M. A. Mega, V. Ribeiro, J. T. R. da Costa Lamelas, E. S. M. M. de Sampaio Nunes, S. R. G. da Silva, A. S. de Teixeira Carrelha, S. C. C. Rodrigues, A. de Figueiredo, M. V. Santos, T. Bilhim, *Radiology* **2021**, *299*, 715.
[52] A. C. C. Esteves, J. Brokken-Zijp, J. Laven, H. P. Huinink, N. J. W. Reuvers, M. P. Van, G. de With, *Polymer* **2009**, *50*, 3955.
[53] O. O. Zaidat, A. J. Yoo, P. Khatri, T. A. Tomsick, R. von Kummer, J. L. Saver, M. P. Marks, S. Prabhakaran, D. F. Kallmes, B. F. Fitzsimmons, J. Mocco, J. M. Wardlaw, S. L. Barnwell, T. G. Jovin, I. Linfante, A. H. Siddiqui, M. J. Alexander, J. A. Hirsch, M. Wintermark, G. Albers, H. H. Woo, D. V. Heck, M. Lev, R. Aviv, W. Hacke, S. Warach, J. Broderick, C. P. Derdeyn, A. Furlan, R. G. Nogueira, et al., *Stroke* **2013**, *44*, 2650.